Journal of the Serbian Chemical Society
JSCS@tmf.bg.ac.rs • www.shd.org.rs/JSCS
J. Serb. Chem. Soc. 90 (5) 623–637 (2025)
JSCS–5410
Original scientific paper
Published 5 June, 2025

Synthesis and characterization of nano $Fe_2CuAl_2O_7$ as a reusable catalyst for Biginelli reaction

MARZIEH M. KESHTIBAN[1], ABBAS NIKOO[2]* and BAKHSHALI MASSOUMI[1]**

[1]*Department of Chemistry, Payame Noor University, Tehran, Iran and* [2]*Department of Organic Chemistry, Faculty of Chemistry, Urmia University, Urmia, Iran*

(Received 8 August, revised 25 September 2024, accepted 10 January 2025)

Abstract: In this research, the novel mixed metal oxide nanoparticles (NPs) $Fe_2CuAl_2O_7$ were synthesized by applying sol-gel auto-combustion method. The $Fe_2CuAl_2O_7$ NPs were identified by XRD, FT-IR, Mapping and EDS. The XRD pattern showed that $Fe_2CuAl_2O_7$ NPs contain a crystalline structure and have just one phase, and types of crystals are FCC. The size distribution of $Fe_2CuAl_2O_7$ NPs was determined by FESEM to be about 41.44 nm. Using the BET equation, the surface area of $Fe_2CuAl_2O_7$ NPs was calculated as 26.174 $m^2\ g^{-1}$. $Fe_2CuAl_2O_7$ NPs were used as a catalyst for the Biginelli reaction. 3,4--Dihydropyrimidine-2(1*H*)-one/thione derivatives were prepared in the presence of $Fe_2CuAl_2O_7$ nanocatalyst with short time and 75–97 % efficiency in water. In addition, the recovery and the reuse of the $Fe_2CuAl_2O_7$ nanocatalyst was done up to five times without significant change in catalytic ability.

Keywords: sol–gel auto-combustion; mixed metal oxides; BET; nanocatalyst; one-pot synthesis.

INTRODUCTION

Mixed metal nano-oxides have attracted special attention of researchers in the nano field due to their unique attributes in terms of properties, structure, and applications.[1] Properties such as electrical,[2] dielectric,[3] magnetic,[4] optical,[5] redox[6] and Lewis acid base behaviour[7] that are of interest. The most widely used fields of these materials are targeted drug delivery,[8] productions of antibacterial,[9,10] superhydrophobic textiles,[11] insecticides,[12] gas storage,[13] batteries,[14] sensors[15] and nanocatalysts.[16–20] Aligning the synthesis of nanocatalysts and green chemistry is a big challenge that chemical scientists have managed well and achieved good success in recent years. Mixed metal nano oxides are one of the types of nanocatalysts that are used as support phase[21] or active phase[22] in

* Corresponding authors. E-mail: a.nikoo@urmia.ac.ir, **b_massoumi@pnu.ac.ir
https://doi.org/10.2298/JSC240808006K

various organic reactions. Mixed metal nano oxides can be used for the oxidation[23] and reduction[24] of organic compounds, the combustion of hydrocarbons,[25,26] the synthesis of widely used chemicals in the industry,[27] biodiesel production[28] and Claisen–Schmidt condensation.[29] The attributed the catalytic properties of oxide surfaces to Lewis acid and base in such a way that Lewis bases are the same oxygens that gather electrons around them, and Lewis acids are metal cations. Also, the defects created on the surface of oxides have a decisive task in their catalytic performance. In general, mixed metal oxides have a crystal structure that depends on the calcination temperature and the synthesis method used for their preparation.[30,31]

The basic structure of many molecules that have medicinal activity such as anticancer, antibacterial, antiviral, antipyretic, and anti-inflammatory as well as fungicidal are heterocyclic compounds.[32] Among numerous heterocyclic compounds, dihydropyrimidines are the most demanding fields of research due to their extraordinary therapeutic and medicinal properties such as cardiovascular drugs,[33] anti-cancers,[34] blood pressure drugs[35] and anti-inflammatory agents.[36] The first compound was synthesized by Biginelli from the three-component one-pot reaction of urea, aldehyde and ketoester in the presence of acid but with low efficiency. During the last decades, various types of catalysts have been reported for this reaction. Among the catalysts can be mentioned such as polymer-immobilized reagents,[37] caffeine,[38] silicotungstic acid supported on Ambelyst-15,[39] mesoporous $NH_4H_2PO_4$/MCM-4,[40] $Fe_3O4@SiO_2$,[41] NiO nanocatalyst[42] and nano-ZrO_2 sulfuric acid.[43] In addition to the advantages, these catalysts suffer from a series of negative features such as low efficiency, use of expensive and toxic solvents, complex conditions for separation, harsh reaction conditions, or sometimes long reaction times. Therefore, it is very important to use a catalyst that performs this profitable reaction with greater efficiency, shorter time, less cost, and less damage to the environment.

In this research, 3,4-dihydropyrimidine-2(1*H*)-one/thione derivatives were synthesized from the one-pot reaction of ethyl acetoacetate, urea or thiourea, and aromatic aldehyde in the presence of the $Fe_2CuAl_2O_7$ heterogeneous nanocatalysts under green and easy conditions.

Integrating atoms or molecules, which is considered a kind of bottom-up approach and is also known as molecular technology, is possible by sol-gel auto-combustion method.[44] To synthesis of pure $Fe_2CuAl_2O_7$ with high level of homogeneity and appropriate size, sol–gel auto-combustion method is a technique that has the advantages of sol–gel and combustion together. This process starts by preparing a solution of metal nitrates in water and sol particles are formed by adding a fuel source such as citric acid. After a heating step, the sol turns into a gel which is a foam-shaped and bulky powder. $Fe_2CuAl_2O_7$ NPs are synthesized by the combustion process with homogenous particles, high purity

percentage and larger surface area. This procedure is an environmentally friendly method, due to the release of CO_2, H_2O and N_2 gases.[45] An uncomplicated preparation procedure, cheap, and commercially available raw materials for the synthesis of $Fe_2CuAl_2O_7$ nanocatalysts are the advantages of this method. The $Fe_2CuAl_2O_7$ nanocatalysts can be recycled up to five stages without reducing its efficiency. The reaction yield and the purity of the products were excellent without the need for complicated separation methods. Researches in various literature showed that the synthesis of the $Fe_2CuAl_2O_7$ nanocatalysts and its application in the preparation of dihydropyrimidines are reported for the first time. The synthesized catalyst has a high stability for a long time, and it has a good durability in the conditions of humidity, heat, and in the open air.

EXPERIMENTAL

Materials

Benzaldehyde derivatives, ethyl acetoacetate, urea, thiourea, citric acid, $Al(NO_3)_3{\cdot}9H_2O$, $Cu(NO_3)_2{\cdot}3H_2O$, $Fe(NO_3)_3{\cdot}9H_2O$ and the solvents were purchased from reputable companies, and were used without the need for purification.

Synthesis of $Fe_2CuAl_2O_7$ NPs

At first, in 1000 ml of distilled water 20.20 g (50 mmol) of $Fe(NO_3)_3{\cdot}9H_2O$, 18.75 g (50 mmol) of $Al(NO_3)_3{\cdot}9H_2O$ and 6.05 g (25 mmol) of $Cu(NO_3)_2{\cdot}3H_2O$ were dissolved. Then, in 250 ml of distilled water 47.13 g (245 mmol) of Citric acid was dissolved and added to the previous mixture. After 3 h stirring the reaction mixture, a sol was formed. A gel formation occurred by water evaporation. The obtained gel was heated overnight at 120 °C by an oven and completely dried. The formed xerogel was calcined in air at 700 °C for 1 h.

*Preparation of 3,4-dihydropyrimidine-2(1*H*)-ones/thiones*

A mixture of ethyl acetoacetate (2.5 mmol, 325 mg), benzaldehyde derivatives (2.5 mmol), urea or thiourea (3.75 mmol), and $Fe_2CuAl_2O_7$ nanocatalyst (0.5 mmol, 170.6 mg) in distilled water (20 mL) was heated under 100 °C. After the accomplishment of the reaction time, as observed by TLC (ether/*n*-hexane: 1/4), the reaction temperature was down to 25 °C, and to the reaction mixture 25 mL of distilled water was added. The catalyst was detached for use in the subsequent reaction by ordinary centrifugation. The 3,4-dihydropyrimidine-2(1*H*)--ones/thiones were extracted with ethyl acetate (3×30 mL), and the organic phase was dried with anhydrous Na_2SO_4 (5 g). Ethyl acetate was separated from the product under reduced pressure, and 3,4-dihydropyrimidine-2(1*H*)-ones/thiones with 75–97 % yields were afforded by recrystallization of residue from ethanol.

Characterization

D500 diffractometer (Siemens) was employed for the pattern X-ray diffraction (XRD) of particles. The XRD pattern of $Fe_2CuAl_2O_7$ NPs at 25 °C was obtained using Cu$K\alpha$ radiation (λ = 0.154 nm) and with a scanning speed of 2°/min. Data were recorded in the range of 10 to 80° with a scan step of 0.5°/s. The dimensions of $Fe_2CuAl_2O_7$ NPs were determined to be 45.045 nm based on the Debye–Scherrer equation (Table I):

$$D = 0.9\lambda/\beta\cos\theta \quad (1)$$

In the Debye–Scherrer equation, θ is the Bragg angle in °, β is the full width at half maximum peak intensity in rad and λ = 1.54060 Å (in the case of CuKα).

TABLE I. Crystallographic data of $Fe_2CuAl_2O_7$ NPs; crystal system: cubic; space group: Fd-3m; space group number: 227

Peak No.	Peak position, 2θ / °	*FWHM*	Crystallite size, *D* / nm	Avg. *D* / nm
1	30.8955	0.2460	33.49	45.045
2	36.2296	0.1476	56.60	–

The information about the size of the particles and morphology was obtained with the device FESEM, Tescan Mira III (field emission scanning electron microscopy) with an accelerating voltage of 20 kV. X-ray electron dispersive spectroscopy (EDS) using a SAMX detector was used to analyse and determine the relative abundance of elements. Spectroscopy Fourier transforms infrared (FT-IR) in the range of 400–4000 cm^{-1} with a KBr disk was used on a Thermo Avatar spectrometer. The adsorption–desorption isotherms, the surface area, the total pore volume and the mean pore diameter were obtained with a Bel Sorp Mini II device on a Bel Prep Vac II analyser by the multipoint Bronauer–Emmett–Teller (BET) method. The completion of the reaction was observed by thin-layer chromatography (TLC) on precoated Merck silica gel 60 F254 and RP-18 F254 plates. The melting points were measured by open capillary with an Electro thermal 9200 device. The reaction yields were calculated after product isolation.

RESULTS AND DISCUSSION

XRD analysis

Fig. 1 shows the XRD pattern for $Fe_2CuAl_2O_7$ NPs as a function of angle. Table II lists the 2θ (°) and relative intensity of each peak.

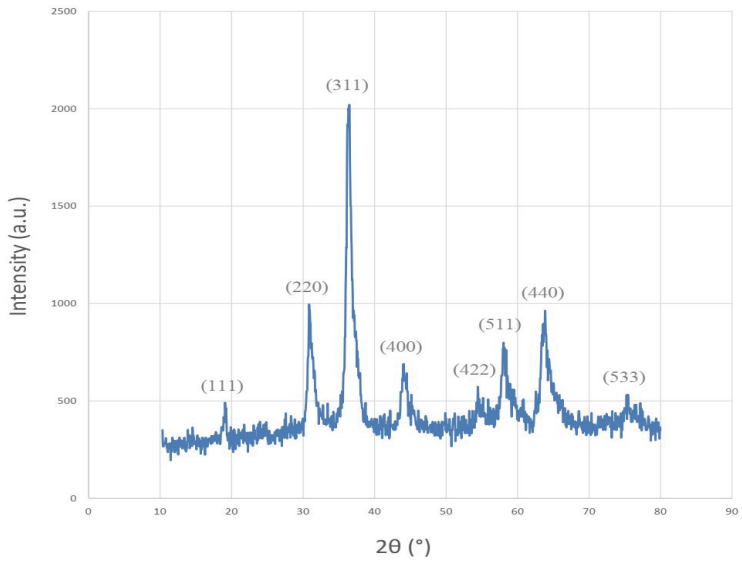

Fig. 1. XRD pattern of $Fe_2CuAl_2O_7$ NPs.

TABLE II. Peak list of $Fe_2CuAl_2O_7$ NPs

Pos. (2θ / °)	Height, cts	*FWHM* Left (2θ / °)	*D*-Spacing, Å	Rel. int., %	Tip width
19.1406	161.58	0.2952	4.63700	11.61	0.3542
30.8955	565.78	0.2460	2.89435	40.67	0.2952
36.2296	1391.21	0.1476	2.47952	100.00	0.1771
44.0461	283.22	0.4920	2.05595	20.36	0.5904
51.0711	56.77	0.2952	1.78842	4.08	0.3542
54.4426	105.93	0.9840	1.68537	7.61	1.1808
57.9885	304.09	0.4920	1.59047	21.86	0.5904
63.4387	335.83	0.3936	1.46633	24.14	0.4723
75.2882	74.89	0.5904	1.26227	5.38	0.7085

The phase determination was done by comparison of the location and intensity of the XRD pattern of $Fe_2CuAl_2O_7$ NPs with references peaks (Fig. 2). The location of the peaks and the relative intensities of the XRD pattern of $Fe_2CuAl_2O_7$ NPs match with the references (Table III).

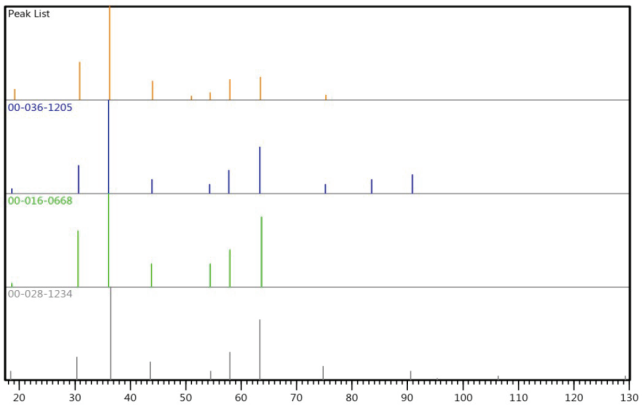

Fig. 2. Plot of identified phases of $Fe_2CuAl_2O_7$ NPs.

TABLE III. Identified patterns list of $Fe_2CuAl_2O_7$ NPs

Ref. code	Score	Compound name	Scale factor	Chemical formula
00-036-1205	65	Cadmium gallium manganese oxide	0.521	$CdMnGaO_4$
00-016-0668	55	Lithium cobalt vanadium oxide	0.420	$LiCoVO_4$
00-028-1234	38	Cobalt chromium iron oxide	0.759	$FeCoCrO_4$

According to the crystal structure of the references mentioned in Table III, the crystal structure of $Fe_2CuAl_2O_7$ NPs is FCC type.

FESEM analysis

FESEM analysis is a microscopic method with high magnification, which was used to investigate the morphology, shape, the surface structure, and the size

distribution of $Fe_2CuAl_2O_7$ NPs in nanometer dimensions (Fig. 3). FESEM image shows that $Fe_2CuAl_2O_7$ NPs are crystalline and homogeneous. According to the FESEM image, the average size of $Fe_2CuAl_2O_7$ NPs is about 41.443 nm.

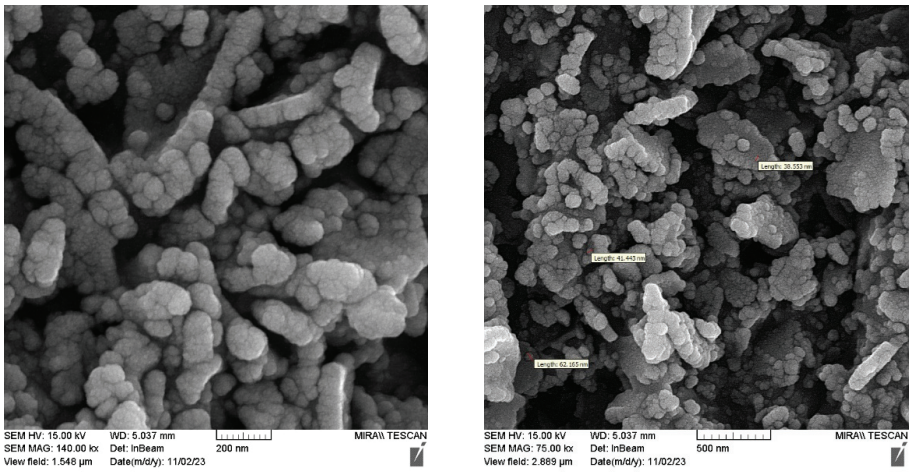

Fig. 3. FESEM images of $Fe_2CuAl_2O_7$ NPs.

EDS analysis

EDS was used to specify the stoichiometry (chemical composition of nanoparticles) and to determine the chemical purity of them (Figs. 4 and 5). The results showed that the only main elements were Fe, Cu, Al and O, respectively, with wt. % of 35.37, 17.39, 18 and 29.24 as well as by the ratio of the number of atoms 18.62, 8.05, 19.61 and 53.72. According to the obtained percentages, the molecular formula of $Fe_2CuAl_2O_7$ was confirmed.

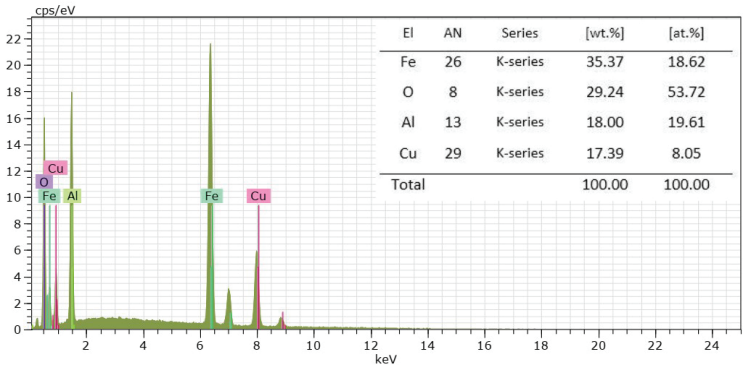

Fig. 4. EDS spectrum of $Fe_2CuAl_2O_7$ NPs.

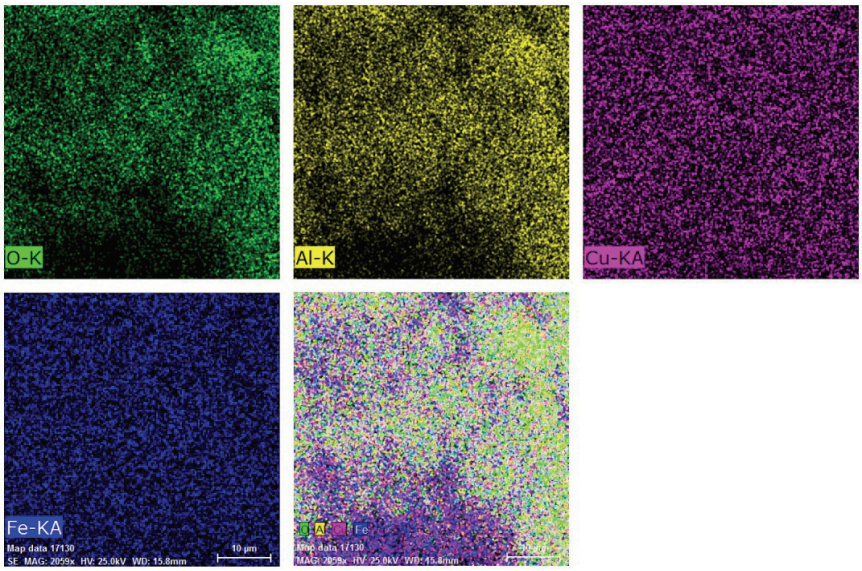

Fig. 5. Mapping data of $Fe_2CuAl_2O_7$ NPs.

Mapping analysis

In concentrated mapping analysis, a particular region of $Fe_2CuAl_2O_7$ NPs was investigated. In mapping analysis was taken from many points in a particular region, and the results of this analysis were represented as a series of coloured points, where each colour represents an element (Fig. 5). Considering that there was a strong bond between the elements, which stayed together and clearly showed the homogeneous distribution of Fe, Cu, Al and O elements according to the molar ratios throughout the structure.

FT-IR analysis

The FT-IR spectrum of $Fe_2CuAl_2O_7$ NPs is shown in Fig. 6. In this spectrum, the broad peak that appeared in the bounds of 3447 cm^{-1} is related to the absorbed water in the stretching state of it. The stretching vibration of the M–O band is at 1637 cm^{-1}, whenever the bending vibration is at 580 cm^{-1}.

Textural analysis

N_2 adsorption–desorption isotherms were used to measure the size distribution, surface area and pore volume of $Fe_2CuAl_2O_7$ NPs at 77 K (Fig. 7). The shape of N_2 adsorption–desorption isotherms according to IUPAC classification is type IV, that specifies the mesopore structure of $Fe_2CuAl_2O_7$ NPs. Based on the hysteresis loop (H3), $Fe_2CuAl_2O_7$ NPs have wedge-shaped pores.

$Fe_2CuAl_2O_7$ NPs capacity was determined by the volumetric gas absorption method with Bel Sorp Mini II absorption device. The total volume of pores was cal-

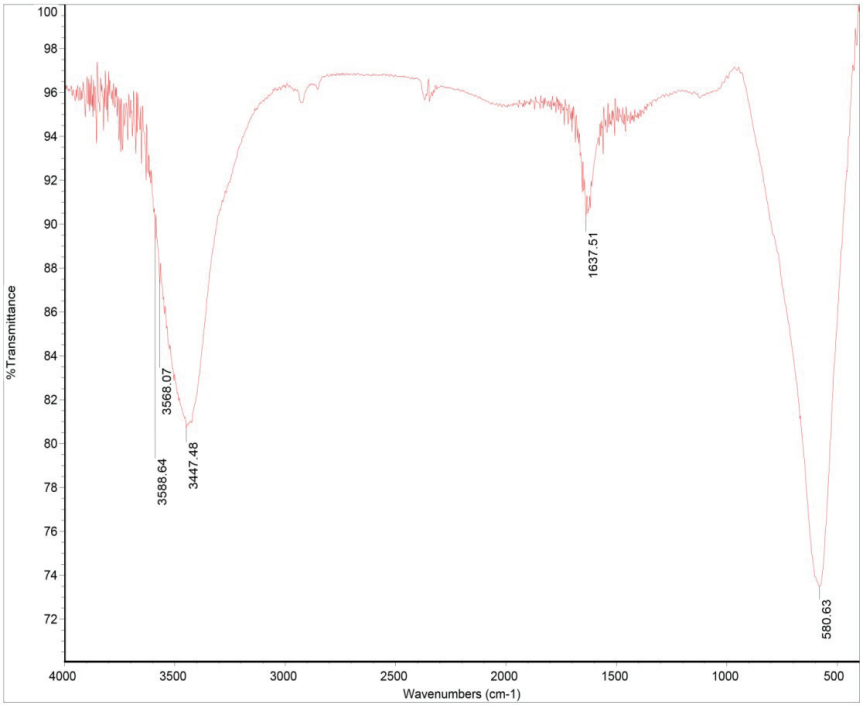

Fig. 6. FT-IR spectrum of $Fe_2CuAl_2O_7$ NPs.

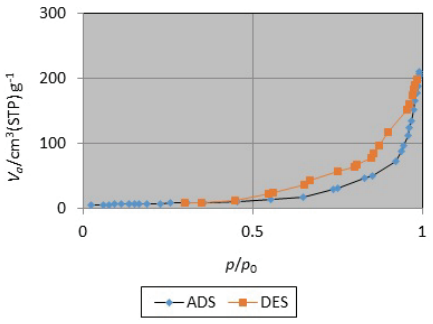

Fig. 7. N_2 adsorption–desorption isotherms of $Fe_2CuAl_2O_7$ NPs.

culated using the amount of nitrogen adsorbed at the highest operating pressure of the experiment. The total surface area was calculated using the BET equation in the initial part of the isotherm (Table IV).

t-Plot (Fig. 8) was used to measure the surface area and volume of pores according to the thickness of gas absorbed on the sample. t-Plot diagram indicating that $Fe_2CuAl_2O_7$ NPs are no microspores because it has no intercept elevation. The mesoporous distribution of the adsorption branch data was performed according to the BJH method. The pore size distribution diagram shows that the pore size is in the range of 2 to 50 nm and the structure of the $Fe_2CuAl_2O_7$ NPs

is completely mesoporous. The pores size distribution curve obtained from the adsorption branch by the BJH method shows that pores with a size of 3.09 nm have the maximum abundance.

TABLE IV. The calculated data of BET, t and BJH plots

Parameter	Value	Unit
	BET-plot	
V_m	6.0135	$cm^3\ g^{-1}$
$a_{s,BET}$	26.174	$m^2\ g^{-1}$
C	167.72	
Total pore volume (p/p_0 = 0.990)	0.3241	$cm^3\ g^{-1}$
Mean pore diameter	49.527	nm
	t-Plot, adsorption branch	
a_1	27.834	$m^2\ g^{-1}$
V_1	0	$cm^3\ g^{-1}$
	BJH-Plot, adsorption branch	
V_p	0.3316	$cm^3\ g^{-1}$
$r_{p,peak}$	3.09	nm
a_p	49.485	$m^2\ g^{-1}$

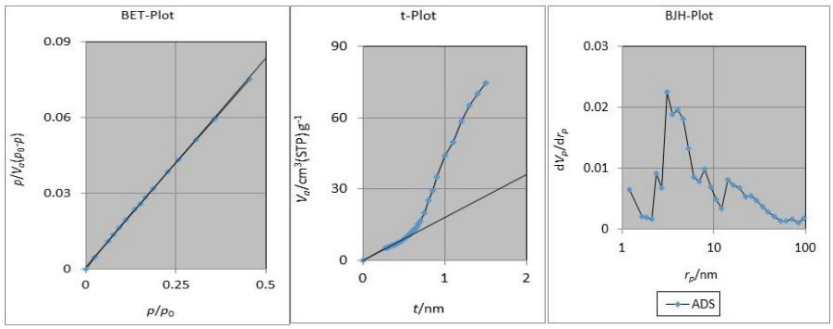

Fig. 8. a) BET plot, b) t-plot and c) BJH plot of $Fe_2CuAl_2O_7$ NPs.

$Fe_2CuAl_2O_7$ nanocatalyst activity

In the present study, $Fe_2CuAl_2O_7$ NPs were used as a catalyst to produce the 3,4-dihydropyrimidine-2(1H)-ones/thiones in excellent yield (Scheme 1). Due to the hydrophobicity of the catalyst and organic reactants, water as a solvent was used in the reactions at a temperature of 100 °C.

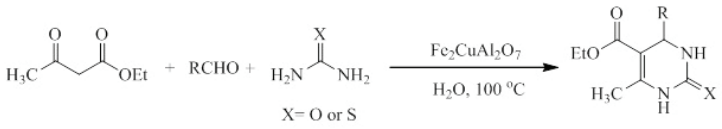

Scheme 1. Synthesis of the 3,4-dihydropyrimidin-2(1*H*)-ones/thiones.

At first, the progress of the reaction was investigated without the $Fe_2CuAl_2O_7$ nanocatalyst. Then, in the presence of different amounts of $Fe_2CuAl_2O_7$ nanocatalyst the reaction efficiency was calculated at the same temperature and time (Table V). The best yield was obtained in the case of using 20 mol % of $Fe_2CuAl_2O_7$ nanocatalyst.

TABLE V. Optimization of $Fe_2CuAl_2O_7$ nanocatalyst; 2.5 mmol benzaldehyde, 2.5 mmol ethyl acetoacetate, 3.75 mmol urea under 100 °C for 90 min

Entry	Catalyst content, mol %	Yield, %
1	–	34
2	10	52
3	15	79
4	20	91
5	25	90
6	30	88

The reaction of other benzaldehydes with electron-withdrawing and electron-donating functional groups were investigated with urea or thiourea and ethyl acetoacetate in order to prepare of the 3,4-dihydropyrimidine-2(1*H*)-ones/ /thiones. All reactions were performed in the presence of $Fe_2CuAl_2O_7$ nanocatalyst using a catalytic amount (20 mol %) in water at 100 °C. The preparation of the 3,4-dihydropyrimidine-2(1*H*)-ones/thiones were obtained in 75–97 % yield (Table VI). According to the information in Table VI, the electron-withdrawing functional groups are effective in the activity of benzaldehyde, however spatial hindrance can reduce the speed and efficiency of the reaction.

A proposed mechanism is presented based on the reactivity of benzaldehyde derivatives for the preparation of the 3,4-dihydropyrimidine-2(1*H*)-ones/thiones (Scheme 2). In the first step, $Fe_2CuAl_2O_7$ nanocatalyst leads to the activation of aldehyde and then ethyl acetoacetate and aldehyde produce intermediate chalcone during aldol condensation in the presence of $Fe_2CuAl_2O_7$ nanocatalyst. Finally, the 3,4-dihydropyrimidine-2(1*H*)-ones/thiones are produced by Michael addition and removal of water by urea or thiourea.

Reusability of the $Fe_2CuAl_2O_7$ nanocatalyst

It was possible to separate and purify the $Fe_2CuAl_2O_7$ nanocatalyst, which is done by filtration or centrifugation. $Fe_2CuAl_2O_7$ nanocatalyst was reused after washing with water, ethanol and ethyl acetate and then drying at 80 °C for 2 h. This process was carried out in five cycles and the reduction of yield was observed from 91 to 84 (7 % reduction of yield during 5 cycles of reaction, Fig. 9). $Fe_2CuAl_2O_7$ nanocatalyst showed excellent stability and activity during 5 consecutive reaction periods. The reaction efficiency shows that the $Fe_2CuAl_2O_7$ nanocatalyst maintains its activity and durability during recycling.

TABLE VI. Synthesis of the 3,4-dihydropyrimidine-2(1*H*)-ones/thiones; 2.5 mmol aldehyde, 2.5 mmol ethyl acetoacetate, 3.75 mmol urea or thiourea and 170.6 mg of $Fe_2CuAl_2O_7$ nano-catalyst in water at 100 °C for 90 min

Entry	R	X	Yield, %	*MP* / °C	
				Found	Reported[46-51]
1	Ph	O	91	202–204	204–206
2	4-Me-Ph	O	81	215–217	214–216
3	4-MeO-Ph	O	85	203–205	201–203
4	2-HO-Ph	O	84	209–211	210–212
5	3-HO-Ph	O	82	170–172	167–170
6	4-HO-Ph	O	75	227–229	230–232
7	2-O_2N-Ph	O	90	220–222	221–222
8	3-O_2N-Ph	O	92	226–228	229–231
9	4-O_2N-Ph	O	94	213–215	211–213
10	4-Cl-Ph	O	92	214–216	215–216
11	Ph	S	92	207–209	205–207
12	4-Me-Ph	S	77	192–194	191–193
13	4-MeO-Ph	S	80	150–152	153–155
14	2-HO-Ph	S	84	203–205	206–208
15	3-HO-Ph	S	93	181–183	183–185
16	4-HO-Ph	S	79	193–195	193–194
17	2-O_2N-Ph	S	95	213–215	215.4–216.4
18	3-O_2N-Ph	S	90	217–219	214–216
19	4-O_2N-Ph	S	97	191–193	190–192
20	4-Cl-Ph	S	91	188–190	192–195

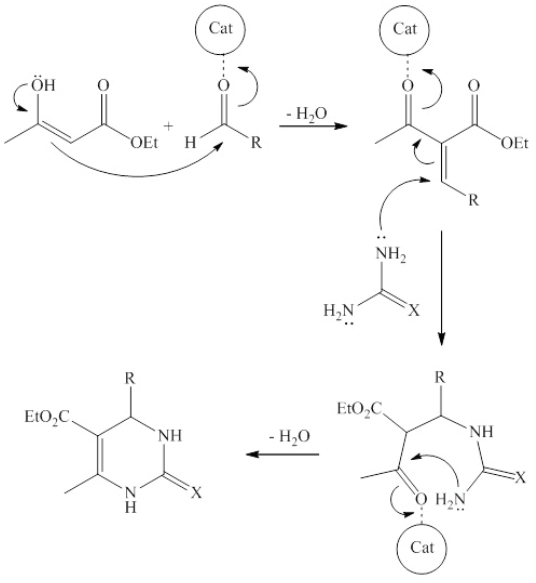

Scheme 2. The suggested mechanism for synthesis of the 3,4-dihydropyrimidin-2(1*H*)-ones/thiones.

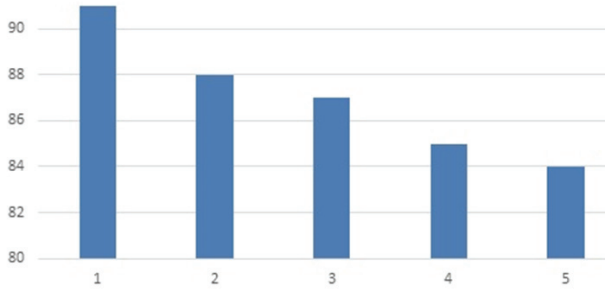

Fig. 9. Reusability of $Fe_2CuAl_2O_7$ nanocatalyst.

CONCLUSION

In this paper, $Fe_2CuAl_2O_7$ NPs were synthesized by sol-gel auto-combustion method. The XRD analysis showed that the crystalline structure of $Fe_2CuAl_2O_7$ NPs is the FCC type. According to the FESEM imaging, the particle size was determined to be about 41.443 nm. Fe, Cu, Al and O elements with ratio 2:1:2:7 were identified in the EDS analysis. The BET analysis showed the surface area of $Fe_2CuAl_2O_7$ nanocatalyst to be 26.174 $m^2\ g^{-1}$. The Biginelli's multicomponent reaction was carried out in the presence of 20 mol % $Fe_2CuAl_2O_7$ nanocatalyst at 100 °C in water as a solvent. The $Fe_2CuAl_2O_7$ nanocatalyst can be recovered and used for at least five periods without a significant decrease in activity. The use of water as the solvent, the short reaction time, the high efficiency and the easy separation of the $Fe_2CuAl_2O_7$ nanocatalyst are the advantages of this method.

Acknowledgment. The authors are grateful to Payam Noor University of Tabriz and Urmia University, Iran, for supporting this research work.

ИЗВОД

СИНТЕЗА И КАРАКТЕРИЗАЦИЈА НАНО $Fe_2CuAl_2O_7$ КАТАЛИЗАТОРА ЗА ВИШЕСТРУКУ УПОТРЕБУ ЗА БИГИНЕЛИЈЕВУ РЕАКЦИЈУ

MARZIEH M. KESHTIBAN[1], ABBAS NIKOO[2] и BAKHSHALI MASSOUMI[1]

[1]*Department of Chemistry, Payame Noor University, Tehran, Iran и* [2]*Department of Organic Chemistry, Faculty of Chemistry, Urmia University, Urmia, Iran*

У овом раду, нове наночестице мешаних металних оксида (NP) $Fe_2CuAl_2O_7$ су синтетисане применом методе сол–гел ауто-сагоревања. $Fe_2CuAl_2O_7$ NP су идентификоване применом следећих техника: XRD, FTIR спектроскопије, мапирања и EDS. Дифрактограми су показали да $Fe_2CuAl_2O_7$ NP имају кристалну структуру и само једну фазу, а кристали површински центрирану кубну решетку. Расподела величина $Fe_2CuAl_2O_7$ NP, одређена FESEM техником, је око 41,44 nm. Применом BET једначине, одређена је специфична површина $Fe_2CuAl_2O_7$ NP: 26,174 $m^2\ g^{-1}$. Синтетисане $Fe_2CuAl_2O_7$ NP су коришћене за Бигинелијеву реакцију. Деривати 3,4-дихидропиримидин-2(1*H*)-он/тиона су добијени у присуству $Fe_2CuAl_2O_7$ нанокатализатора за кратко време и 75–97 % ефикасности у води. Додатно, $Fe_2CuAl_2O_7$ нанокатализатор је успешно коришћен у пет циклуса без значајније промене каталитичких карактеристика.

(Примљено 8. августа, ревидирано 25. септембра 2024, прихваћено 10. јануара 2025)

REFERENCES

1. Đ. Karanović, M. Hadnadjev-Kostic, T. Vulić, M. Milanovic, V. Rajakovic-Ognjanovic, R. Marinkovic-Neducin, J. Serb. Chem. Soc. **89** (2024) 667 (https://doi.org/10.2298/JSC231106005K)
2. P. Kannan, G. Maduraiveeran, *Biosensors* **13** (2023) 542 (https://doi.org/10.3390/bios13050542)
3. R. Lahkale, R. Sadik, W. Elhatimi, F. Z. Bouragba, A. Assekouri, K. Chouni, O. Rhalmi, E. Sabbar, *Physica, B* **626** (2022) 413367 (https://doi.org/10.1016/j.physb.2021.413367)
4. P. K. Boruah, A. Yadav, M. R. Das, *J. Environ. Chem. Eng.* **8** (2020) 104297 (https://doi.org/10.1016/j.jece.2020.104297)
5. A. H. Al-Hammadi, A. Alnehia, A. Al-Sharabi, H. Alnahari, A. B. Al-Odayni, *Sci. Rep*. **13** (2023) 12927 (https://doi.org/10.1038/s41598-023-39845-5)
6. P. M. Malibo, P. R. Makgwane, P. G. Baker, *ChemistrySelect* **5** (2020) 6255 (https://doi.org/10.1002/slct.201904852)
7. T. P. Mabate, N. P. Maqunga, S. Ntshibongo, M. Maumela, N. Bingwa, *SN Appl. Sci.* **5** (2023) 196 (https://doi.org/10.1007/s42452-023-05416-6)
8. S. Saha, M. R. Ali, M. A. Khaleque, M. S. Bacchu, M. A. Aly, M. Z. Khan, *J. Drug Del. Sci. Tech.* **13** (2023) 104728 (https://doi.org/10.1016/j.jddst.2023.104728)
9. D. Paul, A. Pandey, S. Neogi, *World J. Microbiol. Biotechnol.* **39** (2023) 281 (https://doi.org/10.1007/s11274-023-03712-2)
10. K. Kannan, D. Radhika, K. R. Reddy, A. V. Raghu, K. K. Sadasivuni, G. Palani, K. Gurushankar, *Nano Express* **2** (2021) 010014 (https://doi.org/10.1088/2632-959X/abdd87)
11. Y.S. Ko, H. J. Kim, C. W. Ha, C. Lee, *Langmuir* **36** (2020) 11809 (https://doi.org/10.1021/acs.langmuir.0c01515)
12. M. Rahmati, S. Shokri, M. Ahmadi, N. Marvi Moghadam, M. Goodarzi, R. Hazrati--Raziabad, *Plant Biotechnol. Persa* **4** (2022) 79 (http://dx.doi.org/10.52547/pbp.4.1.11)
13. C. Balamurugan, S. J. Song, H. S. Kim, C. Balamurugan, S. J. Song, H. S. Kim, *J. Korean Ceram. Soc*. **55** (2018) 1 (https://doi.org/10.4191/kcers.2018.55.1.10)
14. F. Wu, J. Bai, J. Feng, S. Xiong, *Nanoscale* **7** (2015) 17211 (https://doi.org/10.1039/C5NR04791A)
15. C. S. Lee, J. H. Choi, Y. H. Park, *J. Ind. Eng. Chem*. **29** (2015) 321 (https://doi.org/10.1016/j.jiec.2014.10.048)
16. S. S. Sultana, D. H. Kishore, M. Kuniyil, M. Khan, A. Alwarthan, K. R. Prasad, J. P. Labis, S. F. Adil, *Arab. J. Chem*. **8** (2015) 766 (https://doi.org/10.1016/j.arabjc.2015.05.008)
17. Y. Gao, X. Peng, Z. Zhang, W. Zhang, H. Li, B. Chen, S. Li, Y. Zhang, S. Chi, *Mater. Res. Express.* **8** (2021) 015509 (https://doi.org/10.1088/2053-1591/abdbf7)
18. N. Kumari, S. Kumar, M. Karmacharya, S. Dubbu, T. Kwon, V. Singh, K. H. Chae, A. Kumar, Y. K. Cho, I. S. Lee, *Nano Lett*. **21** (2020) 279 (https://doi.org/10.1021/acs.nanolett.0c03639)
19. N. S. Sarvestani, M. H. Abbaspour-Fard, M. Tabasizadeh, H. Nayebzadeh, T. C. Van, M. Jafari, Z. Ristovski, R. J. Brown, *J. Alloys Compd*. **838** (2020) 155627 (https://doi.org/10.1016/j.jallcom.2020.155627)
20. T. Priamushko, R. Guillet-Nicolas, M. Yu, M. Doyle, C. Weidenthaler, H. Tüysüz, F. Kleitz, *ACS Appl. Energy Mater.* **3** (2020) 5597 (https://doi.org/10.1021/acsaem.0c00544)

21. I. E. Wachs, *Catal. Today* **423** (2023) 113883 (https://doi.org/10.1016/j.cattod.2022.08.025)
22. D. Worch, W. Suprun, R. Gläser, *Chem. Pap.* **68** (2014) 1228 (https://doi.org/10.2478/s11696-013-0533-3)
23. A. M. Kremneva, A. V. Fedorov, O. A. Bulavchenko, Y. V. Knyazev, A. A. Saraev, V. A. Yakovlev, V. V. Kaichev, *Catal. Lett.* **150** (2020) 3377 (https://doi.org/10.1007/s10562-020-03250-8)
24. K. Ichikawa, T. Aoki, M. Akatsuka, M. Yamamoto, T. Tanabe, T. Yoshida, *Catal. Lett*. **154** (2024) 2008 (https://doi.org/10.1007/s10562-023-04424-w)
25. S. K. Singh, H. P. Uppara, P. M. Ramteke, H. Dasari, N. K. Labhasetwar, *Chem. Pap*. **78** (2024) 1805 (https://doi.org/10.1007/s11696-023-03206-3)
26. A. Nau, R. Pointecouteau, M. Richard, T. Belin, F. Can, C. Comminges, N. Bion, *Catal. Commun*. **180** (2023) 106704 (https://doi.org/10.1016/j.catcom.2023.106704)
27. J. Ludvíková, K. Jirátová, F. Kovanda, *Chem. Pap*. **66** (2012) 589 (https://doi.org/10.2478/s11696-011-0127-x)
28. F. Chang, Q. Zhou, H. Pan, X. F. Liu, H. Zhang, W. Xue, S. Yang, *Energy Technol.* **2** (2014) 865 (https://doi.org/10.1002/ente.201402089)
29. S. Toledo-Flores, R. Portillo, G. Del Angel, R. Gómez, *React. Kin. Catal. Lett.* **92** (2007) 361 (https://doi.org/10.1007/s11144-007-5188-z)
30. D. M. Bezerra, E. M. Assaf, *Sci. Technol. Mater.* **30** (2018) 166 (https://doi.org/10.1016/j.stmat.2018.07.001)
31. P. Gerhard, *Phys. Sci. Rev.* **7** (2022) 7 (https://doi.org/10.1515/psr-2020-0183)
32. E. Kabir, M. Uzzaman, *Results Chem*. **4** (2022) 100606 (https://doi.org/10.1016/j.rechem.2022.100606)
33. Y. M. Zohny, S. M. Awad, M. A. Rabie, O. A. Al-Saidan, *Molecules* **28** (2023) 784 (https://doi.org/10.3390/molecules28020784)
34. S. Bijani, D. Iqbal, S. Mirza, V. Jain, S. Jahan, M. Alsaweed, Y. Madkhali, S. A. Alsagaby, S. Banawas, A. Algarni, F. Alrumaihi, *Life* **12** (2022) 519 (https://doi.org/10.3390/life12040519)
35. V. B. Jadhav, H. V. Holla, S. U. Tekale, R. P. Pawar, *Chem. Sin.* **3** (2012) 1213 (https://www.imedpub.com/articles/bioactive-dihydropyrimidines-an-overview.pdf)
36. I. Essid, K. Lahbib, W. Kaminsky, C. B. Nasr, S. Touil, *J. Mol. Struct.* **1142** (2017) 130 (https://doi.org/10.1016/j.molstruc.2017.04.054)
37. N. R. Maurya, A. Patter, D. Singh, K. Ghosh, *Catalysts* **13** (2023) 234 (https://doi.org/10.3390/catal13020234)
38. F. Mohamadpour, M. Lashkari, *J. Serb. Chem. Soc.* **83** (2018) 673 (https://doi.org/10.2298/JSC170712041M)
39. G. Bosica, F. Cachia, R. D. Nittis, N. Mariotti, *Molecules* **26** (2021) 3753 (https://doi.org/10.3390/molecules26123753)
40. R. Tayebee, M. Ghadamgahi, *Arab. J. Chem.* **10** (2017) S757 (https://doi.org/10.1016/j.arabjc.2012.12.001)
41. L. Pirhadi, A. Rangaswamy, E. Soleimani, *Polycyc. Aromat. Comp*. **42** (2022) 4374 (https://doi.org/10.1080/10406638.2021.1891104)
42. M. Khashaei, L. Kafi-Ahmadi, S. Khademinia, A. Poursattar Marjani, E. Nozad, *Sci. Rep*. **12** (2022) 8585 (https://doi.org/10.1038/s41598-022-12589-4)
43. E. Kolvari, N. Koukabi, M. M. Hosseini, M. Vahidian, E. Ghobadi, *RSC Adv.* **6** (2016) 7419 (https://doi.org/10.1039/c5ra19350h)

44. S. Kalpana, V. S. Bhat, G. Hegde, T. N. Prabhu, P. N. Anantharamaiah, *Chem. Pap.* **78** (2024) 343 (https://doi.org/10.1007/s11696-023-03093-8)
45. M. Dara, M. Hassanpour, O. Amiri, M. Baladi, M. Salavati-Niasari, *RSC Adv*. **11** (2021) 26844 (https://doi.org/10.1039/D1RA02609G)
46. Y. Ma, C. Qian, L. Wang, M. Yang, *J. Org. Chem*. **65** (2000) 3864 (https://doi.org/10.1021/jo9919052)
47. R. Zheng, X. Wang, H. Xu, J. Du, *Synth. Commun.* **36** (2006) 1503 (https://doi.org/10.1080/00397910600588488)
48. P. Rajendra, J. Chavan, S. Patel, A. Beldar, V. Shinde, *Chem. J. Mold*. **17** (2022) 101 (https://doi.org/10.19261/cjm.2022.999)
49. F. Rajabi, M. Sillanpää, C. Len, R. Luque, *Catalysts* **12** (2022) 350 (https://doi.org/10.3390/catal12030350)
50. F. Ramezani Gomari, S. Farahi, H. Arvinnezhad, *Iran. J. Chem. Chem. Eng.* **40** (2021) 888 (https://doi.org/10.30492/ijcce.2020.38166)
51. A. Bamoniri, B. B. F. Mirjalili, M. Mahmoodi Fard Chegeni, *J. Nanostruct.* **10** (2020) 751 (https://doi.org/10.22052/JNS.2020.04.0008).